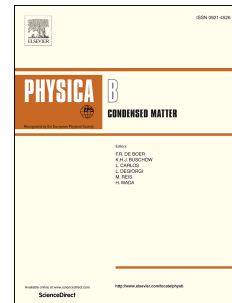


Journal Pre-proof



Detection of Potential Induced Degradation in mono and multi-crystalline silicon photovoltaic modules

I.M. Kwembur, J.L. Crozier McCleland, E.E. van Dyk, F.J. Vorster

PII: S0921-4526(19)30818-X

DOI: <https://doi.org/10.1016/j.physb.2019.411938>

Reference: PHYSB 411938

To appear in: *Physica B: Physics of Condensed Matter*

Received Date: 23 May 2019

Revised Date: 3 December 2019

Accepted Date: 5 December 2019

Please cite this article as: I.M. Kwembur, J.L. Crozier McCleland, E.E. van Dyk, F.J. Vorster, Detection of Potential Induced Degradation in mono and multi-crystalline silicon photovoltaic modules, *Physica B: Physics of Condensed Matter* (2020), doi: <https://doi.org/10.1016/j.physb.2019.411938>.

This is a PDF file of an article that has undergone enhancements after acceptance, such as the addition of a cover page and metadata, and formatting for readability, but it is not yet the definitive version of record. This version will undergo additional copyediting, typesetting and review before it is published in its final form, but we are providing this version to give early visibility of the article. Please note that, during the production process, errors may be discovered which could affect the content, and all legal disclaimers that apply to the journal pertain.

© 2019 Published by Elsevier B.V.

Detection of Potential Induced Degradation in Mono and Multi-Crystalline Silicon Photovoltaic Modules

I.M Kwembur¹, J.L. Crozier McCleland², E.E. van Dyk³, F.J. Vorster⁴

¹ Nelson Mandela University; s215379446@mandela.ac.za

² Nelson Mandela University; Jacqueline.CrozierMcCleland@mandela.ac.za

³ Nelson Mandela University Ernest.vanDyk@mandela.ac.za;

⁴ Nelson Mandela University; Frederik.vorster@mandela.ac.za

Abstract

Potential induced degradation (PID) is a performance limiting defect that profoundly impacts the power output of Photovoltaic (PV) modules. PID occurs because of leakage current between the solar cells and the aluminium frame. The leakage current develops due to high potential difference between the string voltage and the ground. In this work, PID is induced in a mono-crystalline and a multi-crystalline module and the severity is determined by current-voltage (*I-V*) measurements and Electroluminescence (EL) imaging. The Power dropped by 12.6% and 18.7% after 96 hours of PID stress. The extracted parameters from the *I-V* curves show that the shunt resistance decreases and series resistance increases after the induction of PID. EL imaging was done at 10% of short circuit current (I_{sc}) (low injection levels), manifesting as checkerboard like intensity distribution and distinct bimodal intensity histogram. The results of this study demonstrate different PID detection characterisation techniques in PV modules.

Keywords: Potential Induced Degradation (PID), Electroluminescence, Degradation, Shunt Resistance, Series Resistance.

1. Introduction

Photovoltaic (PV) modules convert solar energy to electrical energy and are a proven reliable and sustainable energy source. Over the past decade the number of photovoltaic installations has increased substantially. By 2050, the total PV installation capacity is projected to reach 4.7 TW contributing 16% of the global electricity needs [1,2]. The attainment of the projected global goal may be limited by PV module performance limiting defects such as a phenomenon called Potential Induced Degradation (PID), which has in some cases resulted in up to 14% drop in performance of modules affected by PID [3]. In a PV system, modules are connected in series in order to reach a specified output voltage, typically between 700 V to 1000 V. A potential difference develops between the frame and the cells, leading to a strong electric field that may result in a leakage current flowing between the frame and the cells. Since most PV modules are fabricated from soda lime glass that comprises of 13-14% of Na_2O , Na^+ ions may drift towards the cells due to the electric field. These Na^+ ions will accumulate at the interface between encapsulation and ant-reflecting coating (ARC) and at the right concentration Na^+ ions diffuse into the ARC and eventually into the PN junction resulting in a massive power degradation[4]. The degradation associated with the presence of these Na^+ ions is then termed PID. The PID problem may be compounded further with projected plans for higher string voltages [4]. The extent of PID damage depends on the module construction, ARC, encapsulation used and system design. The formation of PID is linked to the sodium content of the glass cover [5], environmental stresses such as temperature and

humidity play an important role in PID since high humidity encourages moisture ingress through the back sheet of the module. The higher temperature increases the activation energy of Na^+ ions originating from cover glass, contributing to an increase in leakage current [6,7]. In this study, two PV modules, one p-type mono-crystalline and one p-type multi-crystalline silicon were subjected to PID stress by placing them in a conditioned environment ($35^\circ\text{C} \pm 2^\circ\text{C}$ and $70\% \text{RH} \pm 5\% \text{RH}$) while applying the system voltage of 1000 V for 96 hours. The presence of PID was confirmed by dark *I-V* measurements, light *I-V* measurements and Electroluminescence (EL) imaging.

2. Background of characterisation techniques

2.1. Electroluminescence (EL)

Electroluminescence (EL) imaging is a powerful diagnostic tool that is used to determine optical and electronic properties of a module [8,9]. Performance limiting defects such as PID, micro-cracks, cell fractures and defects are ordinarily observable through EL imaging [10,11]. EL is detected when radiative recombination of charge carriers in a semiconductor p-n junction occurs. The intensity of the electroluminescence observed is proportional to the number of available minority charge carriers. A low EL intensity therefore is indicative of the presence of defects in the crystal structure that limit the radiative recombination processes and may have been introduced during cell manufacturing and handling [6]. The EL intensity is proportional to the applied forward voltage, V_f as well as parasitic resistances such as series (R_s) and shunt resistance (R_{sh}). At low current injection levels corresponding to 10% of the module's short circuit current (I_{sc}), PID defects are more distinguishable because of the saturation of carrier recombination centres and shunt current paths. PID develops as a result of more energetic Na^+ ions being forced to diffuse into the silicon crystal structure under the influence of the electric field between the frame and the cells, occupying stacking faults within the original crystallographic structure [4]. PID does not affect all cells in a module or string in the same way due to various leakage current paths and the inhomogeneous distribution of free Na^+ ions within the glass and the encapsulation.

The number of minority carriers responsible for electroluminescence in PID affected cells decreases significantly due to an increase in R_s . The decreased number of minority charge carriers implies that a weak EL signal is detected by the CCD detector and hence the affected cells will appear dark. As the applied voltage increases the number of minority charge currents increases exponentially such that at a current corresponding to I_{sc} the EL intensity of PID affected cells will appear similar to the EL intensity of PID defect free cells. For cells severely affected by PID there is an increase in non-radiative recombination in the PN-junction. These cells will have a very weak EL intensity irrespective of the number of injected carriers. The number of minority carriers is governed by equation (1), where $n_{p(o)}$ is the Excess minority carrier density at the edge of the cell, n_p is the equilibrium minority carrier density in the p layer. e , k , T and V_f are electron charge, the Boltzmann constant, measured temperature and applied forward bias respectively [12].

$$n_{p(o)} = n_p \exp\left(\frac{eV_f}{kT}\right) \quad (1)$$

2.2. Current-Voltage (*I-V*) Characterisation

I-V characteristic curves measured under illumination (light) or in the dark are useful to obtain performance and device parameters. Light *I-V* curves yield performance parameters, viz. open circuit voltage (V_{oc}), short circuit current (I_{sc}), maximum power (P_{mpp}) and the fill factor (FF). Device parameters include dark current (I_o), diode ideality (n) and the parasitic resistances, shunt (R_{sh}) and series (R_s). Dark *I-V* curves may also be used to

estimate series and shunt resistance and diode ideality (n). The deviation from linearity at high voltages on the dark $I-V$ curve represents an increased series resistance while at low voltages increase in slope indicates lower shunt resistance [13,14].

3. Experimental details

3.1. Module Selection

In order to illustrate the effects of PID and apply detection techniques, PID was induced in two p-type modules, a mono-crystalline module (A) and a multi-crystalline module (B). The modules specifications are as listed in Table 1. The PID stress procedure is discussed in section 3.4. The visual inspection of both modules showed no signs of any defects or degradation before and after PID stress. The comparison of performance and device parameters before and after PID stress is presented in the results section.

Table 1

Crystalline Si modules manufacturer specifications.

Module	No. cells	Module size (mm)	V _{oc} (V)	I _{sc} (A)	P _{mpp} (W)
Module A (mono-Si)	72	1200 × 550	46.0	3.61	120
Module B (multi-Si)	72	1956 × 992	45.2	8.95	295

3.2. Electroluminescence

The EL setup comprises of a Si CCD (Silicon Charged Couple Device) camera used to capture the EL image, a programmable power supply to apply the required current in forward bias to the module and a computer with LabVIEW software [15]. The EL setup is such that the module under test and the CCD camera are positioned in a dark enclosure to eliminate the effect of stray light. Fig. 1 shows a schematic diagram of the EL setup used.

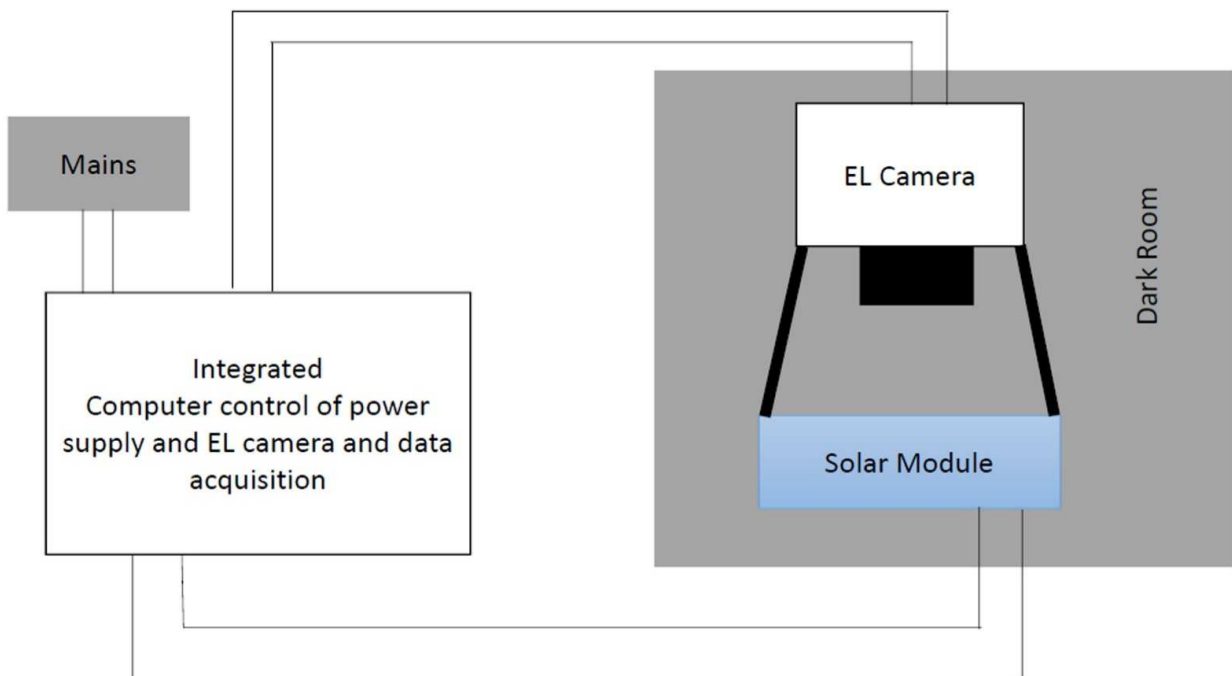


Fig. 1. Schematic set up of an EL imaging

3.3. Current - Voltage (*I-V*) Measurements

Dark current and voltage are measured simultaneously using two Agilent 34401A digital multi-meters while biasing the module from 0 V and 48 V using a programmable power supply. Light *I-V* curve measurements were done using a AAA rated solar simulator under Standard Test Conditions (STC: Temperature 25 °C, and Irradiance of 1000 W/m² with an Air Mass (AM 1.5).

3.4. PID induction procedure

EL imaging, as well as light and dark *I-V* measurements were done on the module A and module B before and after the modules were subjected to PID stress testing according to IEC 62804-1:2015 [16]. The PID stress test was carried out in a controlled environment with the temperature maintained at 35 °C (± 2 °C) and humidity at 70% RH (± 5 % RH) for a period of 96 hours. The module under test was biased at +1000 V using a Chroma electrical safety analyser (19032-P). The positive terminal was connected to the frame while the module's terminals were short circuited and connected to the negative terminal. The leakage current between the frame and module's terminals was monitored throughout the experiment.

4. Results and discussions

4.1 Light *I-V* curves

Fig. 2a) and Fig. 2c) shows light *I-V* curves measured of Modules A and B, before and after PID stress. The decrease in P_{mpp} , and FF are illustrated by the changing shape of the light *I-V* curve at P_{mpp} region. The changing slope at V_{oc} indicates an increase in R_s .

Table 2 is a summary of the PV modules' performance and selected device parameters extracted from the light *I-V* curves before and after the PID stress test. The series and shunt resistances in Table 2 were obtained from the reciprocal of slope near V_{oc} and I_{sc} , respectively. The R_s increases in both module A and module B as a result of a reduction in mobility of charge carriers after PID stress [17,18]. R_{sh} in both modules decreases after PID stress, which may be attributed to presence of Na⁺ which are responsible for increased non-radiative carrier recombination as well as an increase in leakage current paths. P_{mpp} decreased by 12.6% for module A and 18.7% for module B which indicates the severe effect of PID on a module's performance. The increase in ideality coefficient, n , indicates an increase in saturation currents.

4.2 Dark *I-V* curves

The dark *I-V* measurements were taken while the module under test was at room temperature (20 °C to 25 °C) in the dark. The region where R_{sh} dominates in the dark *I-V* curves was identified as 0-5 V while R_s dominates between 40-48 V. The reciprocal of the tangent gradients were obtained as indicated in Fig. 2b) and 2d). In Fig. 2b) the obtained R_{sh} decreases from 4.3 Ω to 2.8 Ω while R_s increased from 7.9 Ω to 13.4 Ω. In Fig. 2d) R_{sh} decreased from 2.7 Ω to 2.5 Ω while R_s increased from 8.3 Ω to 11.6 Ω. This result confirms that R_{sh} decreases after PID stress while R_s increases as was observed in light IV curves, reported in Table 2. PID shunted modules can then be observed on the dark *I-V* measurements as follows: increase in steepness at low voltages indicating decreased R_{sh} . At high voltages the tangent becomes less steep to indicate increasing R_s .

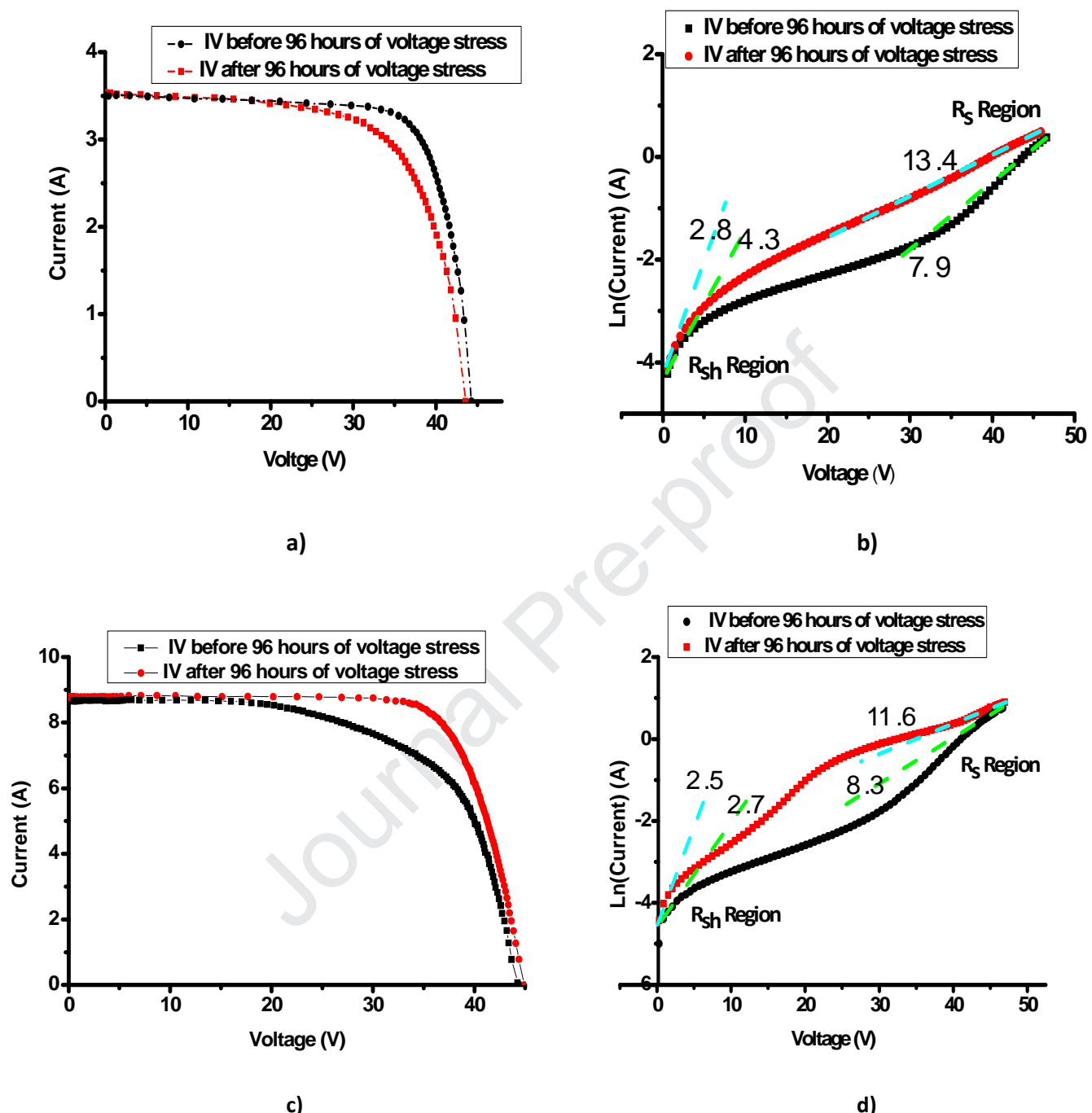


Fig. 2. I - V characteristics of modules before and after PID Stress: a) Light I - V Curve of Module A. b) Dark I - V Curve Module A. c) Light I - V Curve of Module B. d) Dark I - V Curve of Module B. The values indicated in b and d are reciprocals of the respective tangents in Ω units.

Table 2

Light I-V parameters for PV module A and B before and after 96 hours of PID stress at applied bias of 1000V.

Module		V _{oc}	I _{sc}	P _{mpp}	FF	R _{sh} (Ω)	R _s (Ω)	n	% increase in n
A	Before PID	44.31	3.49	116.99	0.76	10000.00	1.25	1.14	39.47
	After PID	43.61	3.53	102.24	0.66	175.43	1.66	1.59	
B	Before PID	44.93	8.78	295.94	0.75	1111.11	0.54	1.45	35.17
	After PID	44.30	8.66	240.58	0.63	133.33	0.73	1.96	

4.3. EL Imaging.

EL images that were taken before and after PID induction and their normalized EL intensity histograms are shown in Fig. 3 and Fig. 4 for modules A and B, respectively. Image histograms plot the frequency distribution of the normalized EL intensities of the EL image. Images a) and b) are taken at a current corresponding to I_{sc}, while EL images c) were taken at a current corresponding to 10% of I_{sc} after the PID stress.

For module A, cell cracks and impurities or manufacturing defects are visible in Fig. 3a) and b). Fig. 3b) shows several cells (M, N and O) that are darker than the rest, a sign that these cells have degraded. However at higher EL intensity corresponding to I_{sc}, it is difficult to identify cells that have undergone less degradation (X, Y and Z). In Fig. 3c), EL image taken at current corresponding to 10% of I_{sc} exhibits overall lower luminescent intensity, the cells appear darker and it is easier to identify cells that have undergone degradation. It is also then possible to distinguish affected cells that are at different stages of PID degradation based on the degree of darkness.

In Fig. 4, the EL image of module B taken at a current corresponding to I_{sc} after PID stress does not show presence of PID affected cells clearly. However, the EL image taken at a current corresponding to 10% of I_{sc} shows several cells in column J and L as well as cell K and others along the frame that have degraded. The cells along the frame are affected more than other cells because the frame is biased to +1000 V and as a result of increased conductivity of the cover glass due to the elevated humidity during the test.

The normalized EL intensity histograms show a distribution based on the electroluminescence intensity level of all the cells. In Fig. 3a) and b) two peaks are observed. The lower intensity peak being visibly smaller representing dark areas on the images as a result of bus bars, manufacturing defects and inter-cell spaces. The lower EL intensity peak in Fig. 3b) broadens because it also includes cells adversely affected by PID shunting. However, the presence of all PID affected cells in Fig. 3b) is difficult to detect since the EL intensity of some PID affected cells also appear masked in the higher intensity peak of the histogram in Fig. 3b). In the histogram of the low injection (taken at current corresponding to 10% of I_{sc}) EL image of Fig. 3c), the single high intensity peak of Fig. 3b) is resolved into two notable peaks. The low intensity peak observed at ≈ 0.15 normalized EL intensity of Fig. 3b) is more pronounced in Fig. 3c) and includes PID affected cells that are more pronounced at low injection levels as a result of the increased relative effect of shunt currents and increased R_s. The middle intensity peak observed at ≈ 0.5 normalized EL intensity in Fig. 3c) represents cells least affected by PID and the high intensity EL peak observed at ≈ 0.75 normalized EL intensity represent cells not affected by PID.

The image histograms for the EL images for module B shows a single unresolved peak in Fig. 4a) and Fig. 4b) which is often mistaken to confirm absence of detectable PID affected cells. The low injection EL histogram of Fig. 4c) shows two distinct peaks. The low intensity peak observed at ≈ 0.15 normalized EL intensity represents PID affected cells along the PV module frame. The second distinct peak observed at ≈ 0.7 normalized EL intensity represent cells that were not affected by PID with the majority occurring at the centre of the module.

The clear bimodal distribution of the EL intensity histogram in Fig. 3c) verifies the value of low injection EL images when the relative effect of low injection currents do not overshadow the detection of PID affected cells. This study confirms the importance of using low injection EL images of modules, recorded at a current corresponding to 10% of I_{sc} and their corresponding histograms as an accurate and a reliable means of PID detection.

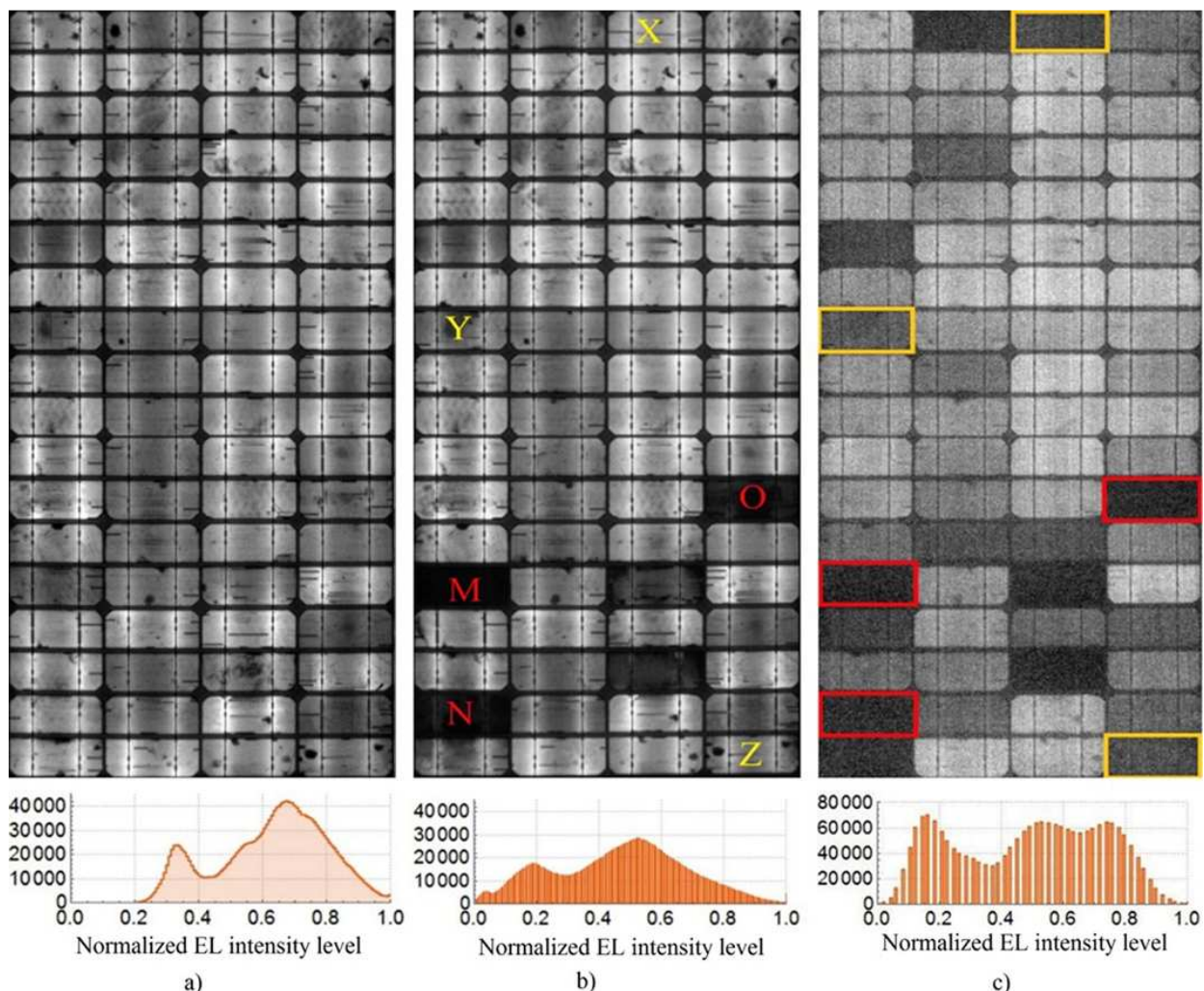


Fig. 3. EL image and intensity histograms of module A. The EL images were obtained as follows: a) Before PID, I_{sc} EL image and image histogram, b) After PID, I_{sc} EL image and image histogram and c) After PID, 10% I_{sc} EL image and image histogram. The I_{sc} of the module is 3.61A.

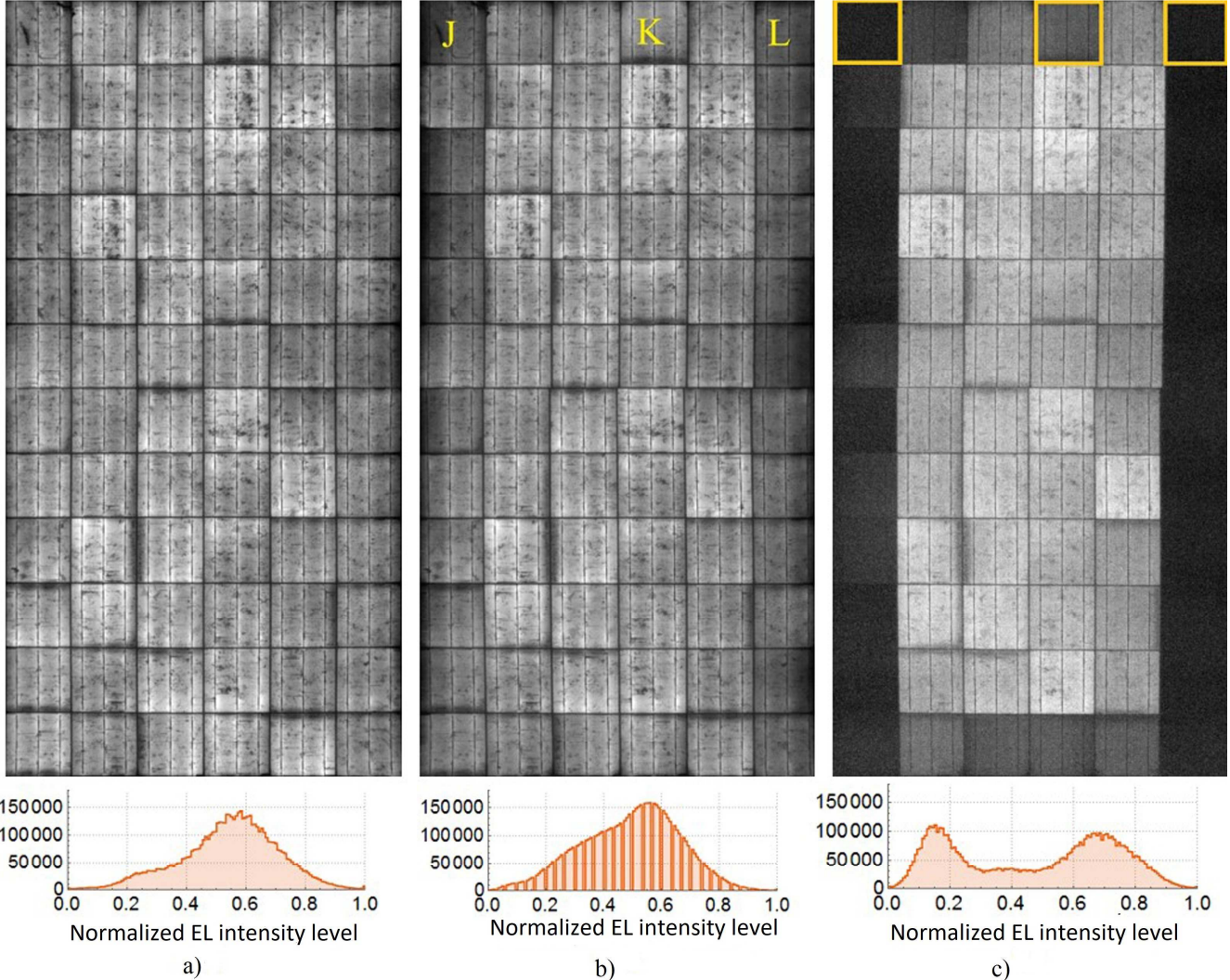


Fig. 4. EL image and intensity histograms of module B. The EL images were obtained as follows: a) Before PID, I_{sc} EL image and image histogram, b) After PID, I_{sc} EL image and image histogram and c) After PID, 10% I_{sc} EL image and image histogram. The I_{sc} of the module is 8.95A.

5. Conclusion

PID was successfully induced and detected in the two PV modules. The extracted module parameters from light $I-V$ curves before and after PID stress such as P_{mpp} , FF, R_{sh} decreased significantly while R_s and n increased in both modules. The decrease in R_{sh} is caused by heavy shunting current due to the accumulation of Na^+ ions on the surface of the cells, making such cells appear darker than the rest on an EL image. Increased R_s after PID stress limits the number of minority charge carriers into the PN junction resulting in the electroluminescence image appearing darker. The EL image of cells taken at a current corresponding to 10% of I_{sc} appear darker. Since each cell in a module will have an R_s increase commensurate to shunting, the EL intensity levels of these darker cell will differ correspondingly. Darker cells have a high R_s and brighter cells have relatively low R_s , hence the checkerboard pattern and the display of distinguishable bimodal peaks on normalized EL intensity histograms. For an EL image taken at a current corresponding to I_{sc} , the individual cell biases is big enough to overcome R_s resulting in a near uniform EL cells brightness across the module with a single noticeable peak on the normalized EL histogram distribution. The early detection using EL images at 10% of I_{sc} and EL image

histograms can help manage P_{mpp} losses which was shown in this work to drop by 12.6% and 18.7% in module A and B respectively.

Acknowledgements

The authors gratefully acknowledge the South African National Research Foundation (NRF), PVinsight (Pty) Ltd, National Laser Centre (NLC), African Laser Centre (ALC), the South African Department of Science and Technology (DST), ESKOM and Nelson Mandela University (NMU) for the financial support and providing necessary facilities for research.

References

- [1] S. Vergura, A complete and simplified datasheet-based model of pv cells in variable environmental conditions for circuit simulation, *Energies.* 9 (2016) 1–12. <https://doi.org/10.3390/en9050326>.
- [2] M. Köntges, S. Kurtz, C. Packard, U. Jahn, K.A. Berger, K. Kato, T. Friesen, H. Liu, M. Van Iseghem, J. Wohlgemuth, D. Miller, M. Kempe, P. Hacke, F. Reil, N. Bogdans, W.H. I, C. Buerhop-Lutz, G. Razongles, and G. Friesen, Review of Failures of Photovoltaic Modules, IEA, 2014. http://iea-pvps.org/fileadmin/dam/intranet/ExCo/IEA-PVPS_T13-01_2014_Review_of_Failures_of_Photovoltaic_Modules_Final.pdf.
- [3] K. Hara, S. Jonai, A. Masuda, Potential-induced degradation in photovoltaic modules based on n-type single crystalline Si solar cells, *Sol. Energy Mater. Sol. Cells.* 140 (2015) 361–365. <https://doi.org/10.1016/j.solmat.2015.04.037>
- [4] W. Luo, Y.S. Khoo, P. Hacke, V. Naumann, D. Lausch, S.P. Harvey, J.P. Singh, J. Chai, Y. Wang, A.G. Aberle, S. Ramakrishna, Potential-induced degradation in photovoltaic modules: A critical review, *Energy Environ. Sci.* 10 (2017) 43–68. <https://doi.org/10.1039/c6ee02271e>
- [5] D. Lausch, V. Naumann, A. Graff, A. Hähnel, C. Hagendorf, J. Bagdahn, Sodium outdiffusion from stacking faults as root cause for the recovery process of potential-induced degradation (PID), *Energy Procedia.* 55 (2014) 486–493. <https://doi.org/10.1016/j.egypro.2014.08.013>
- [6] S. Hoffmann, K. Michael, Effect of humidity and temperature on the potential-induced degradation, *Prog. Photovolt Res. Appl.* 22 (2014) 173–179. <https://doi.org/10.1002/pip.2238>
- [7] SMA corporation, Potential Induced Degradation (PID), 2011. <http://files.sma.de/dl/7418/PID-TI-UEN113410.pdf>.
- [8] F. Fruehauf, M. Turek, Quantification of Electroluminescence Measurements on Modules, *Energy Procedia.* 77 (2015) 63–68. <https://doi.org/10.1016/j.egypro.2015.07.010>
- [9] O. Breitenstein, F. Fr'uhau, D. Hinken, K. Bothe, Effective Diffusion Length and Bulk Saturation Current Density Imaging in Solar Cells by Spectrally Filtered Luminescence Imaging, *IEEE J. Photovoltaics.* 6 (2016) 1243–1254.
- [10] M.A. Islam, M. Hasanuzzaman, N.A. Rahim, A comparative investigation on in-situ and laboratory standard test of the potential induced degradation of crystalline silicon photovoltaic modules, *Renew. Energy.* 127 (2018) 102–113. <https://doi.org/10.1016/j.renene.2018.04.051>
- [11] J. Hylský, D. Strachala, P. Vyroubal, P. Čudek, J. Vaněk, P. Vanýsek, Effect of negative potential on the extent of PID degradation in photovoltaic power plant in a real operation mode, *Microelectron. Reliab.* 85 (2018) 12–18. <https://doi.org/10.1016/j.microrel.2018.04.003>
- [12] International Electrotechnical Commission, Electroluminescence of photovoltaic modules, Geneva, 2019. www.iec.ch.
- [13] E.Q.B. Macabebe, E. Ernest Van Dyk, Extraction of device parameters from dark current-voltage characteristics of PV devices, *Phys. Status Solidi Curr. Top. Solid State Phys.* 5 (2008) 616–619. <https://doi.org/10.1002/pssc.200776834>
- [14] P. Hacke, R. Smith, K. Terwilliger, S. Glick, D. Jordan, S. Johnston, M. Kempe, S. Kurtz, Testing and

- Analysis for Lifetime Prediction of Crystalline Silicon PV Modules Undergoing Degradation by System Voltage Stress, IEEE J. Photovoltaics. 3 (2013) 246–253.
- [15] T. Fuyuki, A. Kitiyanan, Electroluminescence Characterization of Crystalline Silicon Solar Cells, Appl. Phys. A Mater. Sci. Process. 96 (2009) 189–196. <https://doi.org/10.1007/s00339-008-4986-0>.
- [16] IEC, IEC 62804: Photovoltaic (PV) modules - Test methods for the detection of potential-induced degradation - Part 1: Crystalline silicon, (2015) 1–20. <https://webstore.iec.ch/publication/23071>.
- [17] W. Lu, Z. Wang, H. Hu, Polarization effects and tests for crystalline silicon solar cells, J. Semicond. 36 (2015). <https://doi.org/10.1088/1674-4926/36/9/092002>
- [18] S. Sergiu, H. Parikh, P. Hacke, G.A. dos R. Benatto, D. Sera, P.B. Poulsen, Quantification of Solar Cell Failure Signatures Based on Statistical Analysis of Electroluminescence Images, in: Proc. 33rd Eur. Photovolt. Sol. Energy Conf. Exhib., 2017: pp. 1466–1472. <https://doi.org/10.4229/EUPVSEC20172017-5CO.8.5>.

Potential induced degradation (PID) is a major performance limiting defects in PV systems. The defect goes undetected until it is at very advanced stage, making it difficult to reverse the shunting already done on a PV module. This work presents PID detection characterization techniques which will enables detection of the PID defect at infancy.

Authors contributions:

I.M Kwembur¹,

(Article writer and carried out the experiments and characterization)

J.L. Crozier McCleland²,

Setting the experimental and procurement of required equipment

Edited and proof read the work and helped in extraction of histograms from the EL images

E.E. van Dyk³,

The principal scientist who sourced for funding of the research. He also proof read the work

F.J. Vorster⁴

Proof read and edited the work and helped in helped discussion of experimental outcomes

Declaration of interests

The authors declare that they have no known competing financial interests or personal relationships that could have appeared to influence the work reported in this paper.

The authors declare the following financial interests/personal relationships which may be considered as potential competing interests:

